Microwave investigation of the phase diagram of hexagonal multiferroic $HoMnO_3$

Julien Camirand Lemyre and Mario Poirier
Département de Physique, Regroupement Québécois sur les Matériaux de Pointe, Université de Sherbrooke, Sherbrooke, Québec, Canada J1K 2R1

Loreynne Pinsard-Gaudart and Alexandre Revcolevschi
ICMMO, Université Paris-Sud, UMR8182-CNRS, 91405 Orsay Cédex, France

(Received 10 December 2008; revised manuscript received 13 February 2009; published 23 March 2009)

Using a microwave cavity perturbation technique at 16.5 GHz, we have investigated the complex dielectric and magnetic susceptibilities of the hexagonal multiferroic manganite $HoMnO_3$. The *c*-axis and *ab*-plane magnetic susceptibilities both appear to be dominated by the contribution of the Ho^{3+} moments below 100 K. Along the same crystal orientations, Debye relaxation effects are found on the dielectric and magnetic-susceptibility functions above 100 K in a temperature range where unconventional magnetic fluctuations associated to the Mn^{3+} moments are known to exist. At low temperatures, anomalies at the various phase transitions are observed on both susceptibility functions. These were investigated in magnetic fields up to 16 T and an *H-T* phase diagram is deduced for the two crystal directions. Along the *c* axis, the diagram is compared with the one found in the literature.

DOI: 10.1103/PhysRevB.79.094423 PACS number(s): 75.47.Np, 75.50.Ee, 75.40.Cx

I. INTRODUCTION

Rare-earth hexagonal manganites RE-MnO_3 (RE=Sc, Y, Er, Ho, Tm, Yb, Lu) are known to exhibit a ferroelectric (FE) order at high temperatures (600–1000 K) and an antiferromagnetic (AFM) order of the manganese spins at much lower temperatures ($T_N \sim 80$ K). The coexistence of these FE and AFM orders has generated many experiments to understand both the fundamental aspects of their coupling and the possibility of their use in unique devices. The Mn^{+3} moments form triangular planar sublattices stacked along the *c* axis of the hexagonal structure (space group $P6_3cm$); neighboring spins are coupled antiferromagnetically via the oxygen ions by superexchange interaction which gives rise to frustration effects and a 120° angle structure.[1] Rare-earth ions can also carry a magnetic moment oriented along the *c* axis; these moments can interact among themselves as they can do with the Mn^{3+} spins and the dielectric polarization. These interactions yield a complex phase diagram whose effects can be observed on several physical properties.

Among these hexagonal RE-MnO_3 compounds, $HoMnO_3$ is particularly interesting since it shows two additional phase transitions below T_N as observed in neutron scattering[2,3] and second-harmonic generation optical experiments.[4,5] These phase transitions signal modifications of the magnetic order of the Mn^{3+} and Ho^{3+} moments in zero external field. The first transition just below 40 K (T_{SR}) implies an in-plane Mn-spin reorientation by 90° changing the magnetic symmetry from $P6_3cm$ to $P6_3c\underline{m}$. At much lower temperatures below ~ 5 K, another modification of the Mn structure yields a $P6_3cm$ symmetry. These two low-temperature transitions are accompanied by a partial or complete ordering of the Ho^{3+} moments which remains to be completely resolved.

Dielectric anomalies at the magnetic phase transitions have been observed on all hexagonal RE-MnO_3 compounds,[6–8] suggesting a coupling between the magnetic and ferroelectric orders. Although a direct coupling between the in-plane staggered magnetization and the *c*-axis polarization is not allowed in the $P6_3cm$ structure,[9] indirect coupling via lattice strain or other secondary effects have been proposed following the observation of dielectric anomalies at all phase transitions in $HoMnO_3$.[10,11] Under the application of a magnetic field along the *c* axis, a complex *H-T* phase diagram was deduced from dielectric anomalies[11] and neutron measurements;[12] a detailed exploration of this diagram was further conducted with magnetic and heat-capacity experiments.[13] A much simpler diagram with the field along the *ab* plane has been deduced from dielectric constant measurements.[14]

The complexity of the *H-T* phase diagram of hexagonal $HoMnO_3$ justifies additional investigation to specify the different phase boundaries and also to characterize the coupling between the ferroelectric, Mn^{3+} and Ho^{3+} magnetic orders. We report here microwave measurements of the complex magnetic susceptibility and dielectric functions of a $HoMnO_3$ single crystal grown by the floating zone method. These functions, measured parallel and perpendicular to the *c* axis, show anomalies at the three zero-field transitions, the Néel temperature $T_N=72$ K, the Mn-spin rotation $T_{SR}=38.2$ K, and Ho ordering temperature $T_c=5$ K. These anomalies have been investigated for different orientations of a static magnetic field up to 16 T relative to the crystal axes. For $H \| c$, differences with the already published phase diagram are observed at low temperatures. When the field is aligned in the *ab* plane, the anomalies are also modified and a different phase diagram is obtained.

II. EXPERIMENT

$HoMnO_3$ single crystals were grown using the standard floating zone technique. Powder x-ray diffraction measurements confirmed that the crystal investigated here has the $P6_3cm$ hexagonal structure at room temperature. A single crystal was then oriented with a back Laue x-ray diffraction technique. A platelet sample of approximate dimensions 4

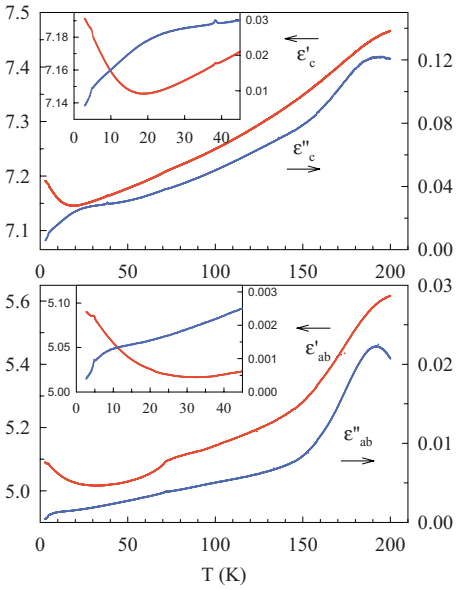

FIG. 1. (Color online) Temperature dependence of the dielectric function in zero magnetic field at 16.5 GHz along the *c* axis (upper panel) and the *ab* plane (lower panel).

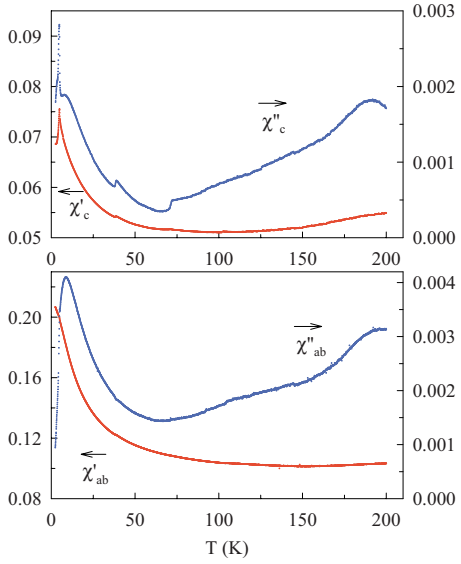

FIG. 2. (Color online) Temperature dependence of the magnetic susceptibility in zero magnetic field at 16.5 GHz along the *c* axis (upper panel) and the *ab* plane (lower panel).

$\times 1.5 \times 1$ mm^3 was cut from the single crystal with the *c* axis oriented along the longest dimension. We used a standard microwave cavity perturbation technique[15] to measure the complex magnetic susceptibility $\chi_k = \chi_k' + i\chi_k''$ and the dielectric function $\epsilon_k = \epsilon_k' + i\epsilon_k''$; the index *k* refers to the *c* axis or to the *ab* plane. A copper cavity resonating in the TE_{102} mode was used at 16.5 GHz. The platelet could then be oriented in the microwave electric or magnetic field by installing it on a quartz rod that can move the sample in and out of the cavity. Following the insertion of the sample, changes in the relative complex resonance frequency $\Delta f/f + i\Delta(1/2Q)$ (Q is the cavity quality factor) could be measured at each temperature between 1.7 and 200 K in a static magnetic field up to 16 T; the data are treated according to the depolarization regime analysis. For the TE_{102} mode at 16.5 GHz, the wavelength ($\sim$2 cm) is much larger than the transverse dimensions of our sample, so no mixing of the electric and magnetic properties occurs. In our experimental setup, the microwave electric field of the cavity is always perpendicular to the static magnetic field, so the field dependence of the dielectric function could not be obtained for $H \| c$. With this microwave technique, the platelet is associated to an ellipsoid and absolute values can only be measured within 30% precision.

III. RESULTS AND DISCUSSION

The dielectric function in zero magnetic field is presented as a function of temperature in Fig. 1. When the temperature is decreased below 200 K, the real part of the dielectric constant ϵ_k' decreases smoothly with a change in rate around 150 K; at lower temperatures, although anomalies are observed at the three phase transitions, it increases rapidly below 20–30 K (see inset). The imaginary part ϵ_k'' shows a wide peak centered around 190 K, then decreases smoothly until 20–30 K and goes rapidly toward zero below 5 K; anomalies at the three phases transitions are also observed. At $T_N = 72$ K, the anomalies are easily observed on ϵ_{ab} (lower panel), when they appear much weaker on ϵ_c (upper panel). At $T_{SR} = 38.2$ K, the situation is reversed: the anomalies are only observed clearly on ϵ_c (see insets). Finally, the rate of increase in the dielectric constant (real part) is modified at $T_c = 5$ K and the losses (imaginary part) goes rapidly toward zero. The presence of these low-temperature anomalies signals a coupling between magnetic and ferroelectric orders both along and perpendicular to the *c* axis. At high temperatures, the features observed around 190 K are consistent with dielectric relaxation effects: the peak on the imaginary part and the increase in the real part, as the temperature is augmented above 150 K, signals a decreasing relaxation time τ of the electric moments at 16.5 GHz; this suggests a value of $\tau > 10^{-11}$ s at low temperatures determined from $\omega\tau = 1$ when maximum dissipation is obtained. These relaxation effects can be purely dielectric or related to magnetic fluctuations arising from the spin liquid phase as revealed in neutron-scattering studies.[3,16–18] Compared to low-frequency measurements,[19] our data along the *c* axis show a similar temperature dependence, but the anomalies are much smaller in amplitude; the main difference is, however, the presence of relaxation effects at both ends of the temperature range. Furthermore, no in-plane dielectric data have been published for this compound. At low temperatures, our dielectric constant shows a temperature dependence which is in close connection with the microwave magnetic susceptibility as will be shown next.

The temperature dependence of the magnetic susceptibility in zero magnetic field is shown in Fig. 2. Along both crystalline directions, the real part first decreases weakly below 200 K (more pronounced along the *c* axis), then goes through a minimum before increasing more rapidly below 50 K. At lower temperatures, a sharp peak at 5 K and a small change in slope are, respectively, observed on χ_c' and χ_{ab}'.

The imaginary part shows a wide maximum near 190 K before decreasing smoothly down to 70 K; at lower temperatures, it increases rapidly and then goes through a maximum around 9 K followed at 5 K by a sharp peak on χ_c'' and a faster decrease on χ_{ab}''. Anomalies at T_{SR} and T_N can also be observed easily on χ_c but with much smaller amplitude on χ_{ab}. The real part of these microwave magnetic susceptibilities below 100 K is similar to superconducting quantum interference device (SQUID) magnetization data,[20] but the anomalies at the different phase transitions are more accentuated. No imaginary parts were ever published at low frequency.

Two main contributions seem to dominate both microwave susceptibilities. At high temperatures ($T>100$ K), relaxation effects mainly revealed by an increase in dissipation (imaginary part) are similar to the one observed on the dielectric function and likely due to magnetic fluctuations of the Mn system; this is compatible with an increasing relaxation time of these fluctuations as the Néel temperature is approached from high temperatures. In $YMnO_3$,[17] these fluctuations originate from short-range dynamic correlations which are a signature of a spin liquid phase arising from geometrical frustration. The magnetic fluctuations could then be correlated with ferroelectric ones via the lattice. Indeed, it has been shown that the in-plane elastic constant C_{11} softens above T_N due to a coupling with magnetic fluctuations.[21] Since it is known that both the dielectric constant and the polarization decrease at the Mn ordering temperature T_N,[19] a decrease in the microwave dielectric constant and of the magnetic susceptibility below 200 K due to these short-range correlations is not surprising. At low temperatures, the increase in the susceptibility is dominated by the magnetism of the Ho system. At $T_c=5$ K, the susceptibility data are consistent with easy axis long-range AFM order of the Ho^{3+} moments: cusp on χ_c' and change in slope on χ_{ab}'. For $T>5$ K, the imaginary part of the susceptibility shows a maximum which can be explained by relaxation effects; indeed, if a monodispersive Debye relaxation model is used for the Ho moments, we can define a temperature dependent relaxation time $\tau_k(T)$ as

$$\tau_k(T) = \frac{\chi_k''}{\omega \chi_k'}. \quad (1)$$

Because the contribution of the Mn^{3+} moments to the overall susceptibility cannot be ignored, it is not possible to extract this relaxation time along both directions. But as it is observed in other magnetic systems[22] when $\omega\tau$ is much less than 1, the temperature dependence of τ is directly revealed by the imaginary part χ_k''. Below 100 K the increasing χ_k'' then initiates a dynamical critical slowing down which is stopped around 9 K where the approach of the three-dimensional (3D) transition temperature T_c speeds up the relaxation time; the speeding up is also highly pronounced below T_c on χ_{ab}'' when the behavior is more complex on χ_c''. Because of the coupling between the Ho^{3+} and Mn^{3+} moments, this dynamical critical slowing down is affected by the 3D ordering of the Mn moments at $T_N=72$ K and at their in-plane rotation transition accompanied by a partial ordering

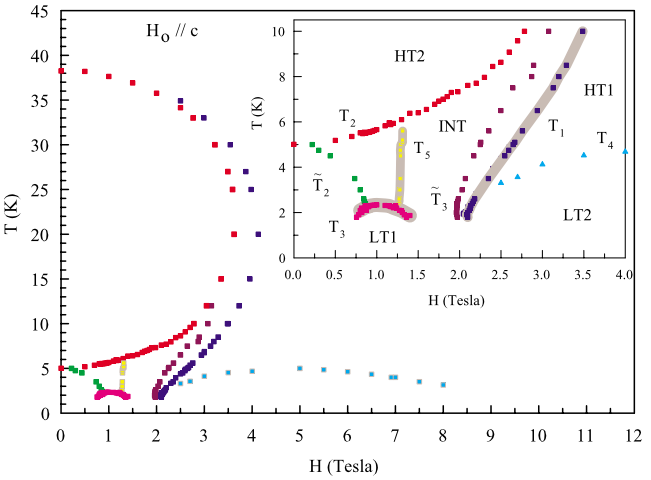

FIG. 3. (Color online) Phase diagram of $HoMnO_3$ for a magnetic field oriented along the c axis. Inset: details of the low-temperature part; the gray lines indicate where hysteresis is found.

of the Ho moments along the c axis at $T_{SR}=38.2$ K. These effects are clearly important along the c axis (Fig. 2 upper panel) but quite weak for the in-plane configuration (lower panel). Moreover, anomalies are revealed most efficiently on the imaginary part of the susceptibility, an observation which is consistent with $\omega\tau \ll 1$ for the Ho moments.

Among all the anomalies identified on the dielectric and magnetic-susceptibility functions at three phase transitions, the ones observed simultaneously on χ_c' and χ_c'' are the most important (Fig. 2) and they have been used to map the magnetic phase diagram shown in Fig. 3 for a field oriented along the c axis. This diagram is similar to the one already published[11,13] for a crystal grown by the flux method, but some differences are clearly identified. To help the comparison, we have adopted the same indexing of the phases and boundaries in the inset of Fig. 3. In zero field, the value $T_c=5$ K is only 0.3 K lower than the reported one,[11] T_{SR} is higher by almost 6 K at 38.2 K (32.8 K), and T_N is lower by 4 K at 72 K (76 K). These values of the zero-field transition temperatures are typical of a crystal grown by the floating zone technique.[19,23] These differences with the other growth method could be interpreted as a stronger Ho^{3+}-Mn^{3+} interaction (higher T_{SR}) and weakened exchange interactions among the same type of moments (smaller T_c and T_N) in relation with oxygen defects. As observed in another compound,[21] the Néel temperature T_N is weakly depressed by a magnetic field of 16 T (0.05 K), and this is why this boundary does not appear on the phase diagram.

In the high-temperature part of the diagram, T_{SR} is progressively depressed without any hint of a splitting into $T_1(H)$ and $T_2(H)$ before the magnetic field has reached 2 T; over this field value, both transitions present a reentrant behavior near 3–4 T and different destinations at low temperatures. The absence of a line splitting at low fields could be related to an increased broadening of the anomalies by oxygen defects. Although the low-temperature part of the diagram (detailed in the inset of Fig. 3) shows similarities with the published one, several differences related to the T_3 dome and the hysteresis effects are also observed. These differ-

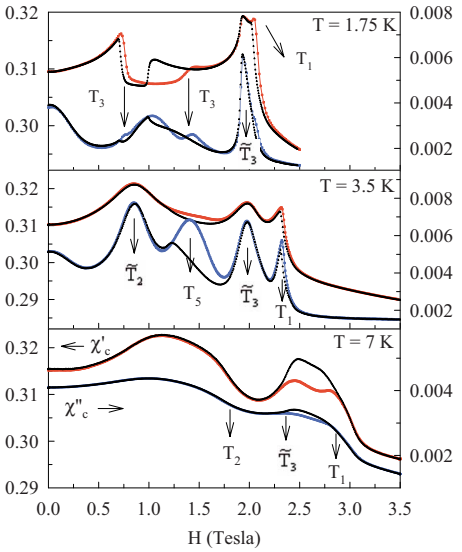

FIG. 4. (Color online) Magnetic field dependence of the susceptibility χ_c at three different temperatures. Curves of increasing field, red and blue (gray), and decreasing field, black. Arrows indicate the phase boundaries.

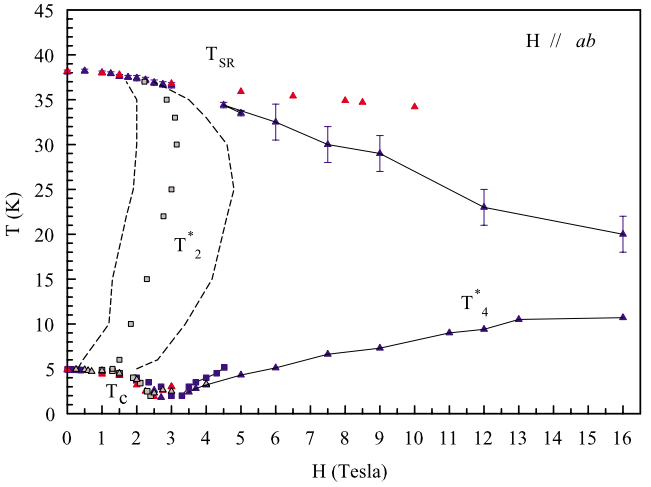

FIG. 5. (Color online) Phase diagram of $HoMnO_3$ for a magnetic field oriented along the *ab* plane. Temperature sweeps (△), field sweeps (□); ϵ_c (red or dark gray), χ_c (blue or black), and χ_{ab} (light gray). The lines indicate the region where hysteresis is found on field sweeps, the solid one indicating the maximum value.

ences are summarized in the field sweeps at fixed temperature shown in Fig. 4. At 1.75 K, four transition lines are identified: the two lines of the T_3 dome, $\tilde{T}_3$ and T_1. From up and down sweeps, hysteresis effects are observed on all lines except $\tilde{T}_3$. At 3.5 K, the T_5 transition appears with three other lines $\tilde{T}_2$, $\tilde{T}_3$, and T_1, and hysteresis is only observed on two lines: important effects for T_5 and small ones for T_1. Finally at 7 K, three lines are observed, T_2, $\tilde{T}_3$, and T_1: if T_2 is free from any hysteresis, it covers now the full region between $\tilde{T}_3$ and T_1. The three boundaries where hysteresis has been observed are indicated as shaded gray lines in the inset of Fig. 3. Only the T_5 boundary hysteresis agrees with the data of Yen *et al.*,[11] hysteresis being rather observed on the T_1 line instead of the $\tilde{T}_3$ one. At low temperatures, hysteresis is confined at T_1 but it spreads progressively to occupy the region between $\tilde{T}_3$ and T_1 as the temperature is increased up to 7–8 K (not shown in Fig. 3); at higher temperatures, the hysteresis decreases, but remains centered on T_1, to finally disappear when $\tilde{T}_3$ merges with T_2 above 10 K. The T_3 dome is also different from the published one: the maximum value $T_3(H)=2.3$ K is 1 K lower and its field extension at 1.75 K (0.75–1.5 T) appears reduced.

The phase diagram shown in Fig. 3 shows very close resemblance with the one deduced from giant magnetoelectric effect on a crystal also grown by an optical floating zone furnace.[19] This is a clear indication that the growth technique used for these hexagonal multiferroics not only affects the zero-field values of the transitions, but it modifies several phase boundaries. The Mn^{3+}-Mn^{3+} and Ho^{3+}-Mn^{3+} interactions are likely the ones mainly affected by oxygen defects. This is relevant information since some experiments require large crystals that can be obtained only with the floating zone method. Finally, it has been suggested by Lorenz *et al.*[13] that four of the five low-temperature phases coexist at a tetracritical point at 2 K and 1.8 T. Our phase diagram does not agree with this picture: only two lines, T_1 and $\tilde{T}_3$, seem to converge toward a common point near 2 T. Only measurements performed at much lower temperatures could clarify this issue in this type of crystal.

A phase diagram with the magnetic field oriented along the *ab* plane is shown in Fig. 5. It was mapped from temperature sweeps at fixed field and field sweeps at fixed temperature from ϵ_c, χ_c, and χ_{ab} anomalies. The field dependence of the Néel temperature T_N (not shown in Fig. 5) is much more accentuated for this field orientation, a 2 K shift in a field of 16 T, a value 40 times greater than along the *c* axis. In the diagram, anomalies that could be followed

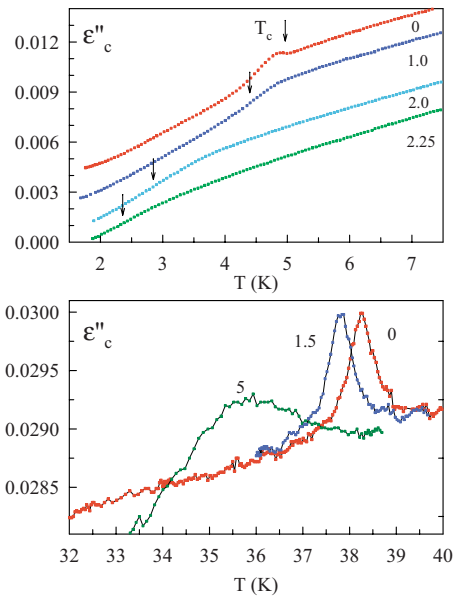

FIG. 6. (Color online) Temperature dependence of ϵ_c'' at different magnetic field (tesla) oriented along the *ab* plane.

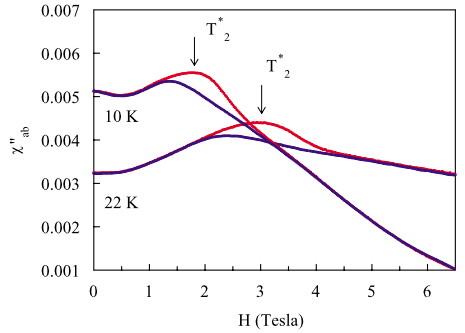

FIG. 7. (Color online) Magnetic field dependence of χ''_{ab} at 10 and 22 K: field oriented along the *ab* plane; curves for increasing and decreasing field, red (gray) and blue (black).

clearly with field are associated to points not related by lines. This is the case of the transition at $T_c=5$ K in zero field: as shown in Fig. 6 (upper panel) on $\epsilon''_c(T)$, for example, the transition is defined in zero field by a kink indicated by an arrow; this kink is rapidly suppressed by the field ($\sim$0.5 T), and the transition rather defined by the maximum slope (indicated by an arrow) is depressed progressively toward zero as the magnetic field increases up to $\sim$2.75 T, an observation fully consistent with previous dielectric measurements.[14] Such a behavior is consistent with a reduction in the in-plane Ho^{+3}-Ho^{+3} AF exchange interaction by a perpendicular magnetic field. The Mn spin-rotation transition at $T_{SR}=38.2$ K is also depressed when the field is increased up to 10 T (lower panel of Fig. 6) where the anomaly becomes vanishingly small; this is again in agreement with published data which show absence of any reentrance for this field orientation.[14] This could be explained by a canting of the Ho moments relative to the *c* axis that weakens the Ho^{3+}-Mn^{3+} interaction. The boundary indicated by points joined by solid lines and deduced from a slope variation on χ_c seems to split from the T_{SR} line above 3 T; whether this apparent splitting represents a true phase boundary remains an open question since it could not be observed on all physical quantities.

Another line T_4^* also associated to a change in slope on χ_c is issued from the point (3 T, 1.75 K) where the T_c boundary disappears; it extends up to 16 T with a value saturating around 10 K. Whether this line represents a true phase boundary or not remains to be clearly established; the coupling of this boundary with ϵ_c and χ_{ab} is probably too weak to be observed. Finally, a line T_2^* is joining the T_c and T_{SR} boundaries in the low-field portion of the diagram. This line is associated to a dissipative process revealed by a maximum on χ''_{ab} when the field is swept at fixed temperatures as shown in Fig. 7. If the maximum indicating T_2^* is clearly shifted for different temperatures, strong hysteresis whose extension is indicated by dashed lines on the phase diagram of Fig. 5 is revealed. In this hysteretic portion of the diagram, slope variations on ϵ_c and χ_c are also observed, but their behavior cannot be coherently related to T_2^*.

For this field orientation, our microwave data confirm the depression of both T_c and T_{SR} already reported in a dielectric measurement[14] and the outcome of new phases involving the Ho moments. However, the other features reported in the diagram remain to be confirmed on other physical properties and on crystals obtained by different growth techniques. Moreover, we should verify any in-plane anisotropy since the exact orientation of the field along the *ab* plane is not known in our microwave experiments.

IV. CONCLUSION

In this paper, we have shown that there is a close connection between microwave dielectric and magnetic-susceptibility functions over the 2–200 K temperature range in the multiferroic $HoMnO_3$. If intralayer magnetic fluctuations of the Mn^{3+} moments seem to contribute to these physical properties above the Néel temperature, the Ho^{3+} moment system dominates completely below T_N due to a short relaxation time. The temperature profile of the magnetic susceptibility along both crystalline directions is fully consistent with a 3D AF ordering of the Ho moments along the *c* axis below 5 K. The imaginary part of the susceptibility, in particular, reflects the process of critical slowing down of the Ho moments when the ordering temperature T_c is approached from high temperatures; the anomalies at T_N and T_{SR} indicate a reduction in the Ho^{3+} moment relaxation time when the magnetic structure is modified. These anomalies have been used to map the *H-T* phase diagram of $HoMnO_3$. Along the *c* axis, the diagram displays some differences with the one published for a crystal grown by the flux method. First, the zero-field values of T_c, T_{SR}, and T_N are shifted consistently with a reduction in the Mn^{3+}-Mn^{3+} exchange interaction and an increase in the Mn^{3+}-Ho^{3+} one due to oxygen defects; then, the $T_3(H,T)$ dome appears reduced, no critical point joining four lines at low temperatures near 2 T can be identified, hysteresis effects are not observed on the same lines, and the splitting of the $T_{SR}(H)$ is not observed below 2.5 T. These differences reflect the importance of the growth technique in the determination of the structure of the multiple phases appearing under the application of a magnetic field. Finally, we have determined the phase diagram for a field oriented along the *ab* plane. We observe not only a reduction in both T_c and T_{SR} with field below 3 T, but the appearance of a hysteretic dome between these two boundaries below 4–5 T. Two other lines have also been deduced at higher field values but complementary measurements are likely needed to confirm their link with phase-transition boundaries.

ACKNOWLEDGMENTS

The authors acknowledge the technical support of Mario Castonguay. This work was supported by grants from the Fonds Québécois de la Recherche sur la Nature et les Technologies (FQRNT) and from the Natural Science and Engineering Research Council of Canada (NSERC).

[1] A. Munoz, J. A. Alonso, M. J. Martinez-Lope, M. T. Casais, J. L. Martinez, and M. T. Fernandez-Diaz, Phys. Rev. B **62**, 9498 (2000).
[2] A. Munoz, J. A. Alonzo, M. J. Martinez-Lope, M. T. Casais, J. L. Martinez, and M. T. Fernandez-Diaz, Chem. Mater. **13**, 1497 (2001).
[3] Th. Lonkai, D. Hohlwein, J. Ihringer, and W. Prandl, Appl. Phys. A: Mater. Sci. Process. **74**, S843 (2002).
[4] M. Fiebig, D. Frohlich, K. Kohn, S. Leute, T. Lottermoser, D. Frölich, V. V. Pavlov, and R. V. Pisarev, Phys. Rev. Lett. **84**, 5620 (2000).
[5] M. Fiebig, C. Degenhardt, and R. V. Pisarev, J. Appl. Phys. **91**, 8867 (2002).
[6] N. Iwata and K. Kohn, J. Phys. Soc. Jpn. **67**, 3318 (1998).
[7] T. Katsufuji, S. Mori, M. Masaki, Y. Moritomo, N. Yamamoto, and H. Takagi, Phys. Rev. B **64**, 104419 (2001).
[8] H. Sugie, N. Iwata, and K. Kohn, J. Phys. Soc. Jpn. **71**, 1558 (2002).
[9] R. R. Birss, *Symmetry and Magnetism* (North-Holland, Amsterdam, 1966).
[10] B. Lorenz, A. P. Litvinchuk, M. M. Gospodinov, and C. W. Chu, Phys. Rev. Lett. **92**, 087204 (2004).
[11] F. Yen, C. R. de la Cruz, B. Lorenz, Y. Y. Sun, Y. Q. Wang, M. M. Gospodinov and C. W. Chu, Phys. Rev. B **71**, 180407(R) (2005).
[12] O. P. Vajk, M. Kenzelmann, J. W. Lynn, S. B. Kim, and S. W. Cheong, Phys. Rev. Lett. **94**, 087601 (2005).
[13] B. Lorenz, F. Yen, M. M. Gospodinov, and C. W. Chu, Phys. Rev. B **71**, 014438 (2005).
[14] R. Vasic, H. D. Zhou, E. Jobiliong, C. R. Wiebe, and J. S. Brooks, Phys. Rev. B **75**, 014436 (2007).
[15] L. Buravov and J. F. Shchegolev, Prib. Tekh. Eksp. **2**, 171 (1971).
[16] T. J. Sato, S. H. Lee, T. Katsufuji, M. Masaki, S. Park, J. R. D. Copley, and H. Takagi, Phys. Rev. B **68**, 014432 (2003).
[17] J. Park, J. G. Park, G. S. Jeon, H. Y. Choi, C. Lee, W. Jo, R. Bewley, K. A. McEwen, and T. G. Perring, Phys. Rev. B **68**, 104426 (2003).
[18] B. Roessli, S. N. Gvasaliya, E. Pomjakushina, and K. Conder, JETP Lett. **81**, 287 (2005).
[19] N. Hur, I. K. Jeong, M. F. Hundley, S. B. Kim, and S.-W. Cheong, arXiv:0805.3289 (unpublished).
[20] E. Galstyan, B. Lorenz, K. S. Martirosyan, F. Yen, Y. Y. Sun, M. M. Gospodinov, and C. W. Chu, J. Phys.: Condens. Matter **20**, 325241 (2008).
[21] M. Poirier, F. Laliberté, L. Pinsard, and A. Revcolevschi, Phys. Rev. B **76**, 174426 (2007).
[22] A. Caillé and M. Poirier, Solid State Commun. **60**, 945 (1986).
[23] D. Talbayev, A. D. LaForge, S. A. Trugman, N. Hur, A. J. Taylor, R. D. Averitt, and D. N. Basov, Phys. Rev. Lett. **101**, 247601 (2008).